




# Cold RF oxygen plasma treatment of graphene oxide films

F. M. El-Hossary<sup>1</sup>, Ahmed Ghitas<sup>2</sup>, A. M. Abd El-Rahman<sup>1,3</sup>, A. A. Ebnalwaleed<sup>4</sup>,  
M. Abdelhamid Shahat<sup>2,\*</sup> , and Mohammed H. Fawey<sup>1</sup>

<sup>1</sup> Physics Department, Faculty of Science, Sohag University, Sohag 82524, Egypt

<sup>2</sup> PV Unit, Solar and Space Research Department, National Research Institute of Astronomy and Geophysics (NRIAG), Helwan 11421, Cairo, Egypt

<sup>3</sup> King AbdulAziz University, Jeddah, Saudi Arabia

<sup>4</sup> Electronics & Nano Devices Lab, Physics Department, Faculty of Science, South Valley University, Qena 83523, Egypt

**Received:** 20 February 2021

**Accepted:** 3 May 2021

**Published online:**  
17 May 2021

© The Author(s), under  
exclusive licence to Springer  
Science+Business Media, LLC,  
part of Springer Nature 2021

## ABSTRACT

Oxygen radio-frequency (RF) plasma technique is one of the most novel directions used to improve the physical and chemical properties of graphene oxide (GO). Herein, plasma treatment is used to enhance the chemical functionalization and reduced levels of the GO material for electronic and solar cell applications. GO films were chemically synthesized with high quality and uniformity. Then, they exposed to surface modification using RF oxygen plasma at a processing power of 100 W at different processing times. The microstructure and surface chemistry of the GO films were characterized by X-ray photoelectron spectroscopy (XPS) and Raman spectroscopy. Moreover, the effect of oxygen plasma on the thermal stability, surface roughness, contact angle, work of adhesion, wettability, spreading coefficient, and electrical properties have been studied. The results revealed a decrease in the amount of oxygen-containing groups (such as epoxides, carbonyls, and carboxyl groups) from 48.8% in pristine GO to 36.15% after 5 min of oxygen plasma treatment. Besides, the carbonyls groups (C = O) disappeared while new chemical bonds were created compared to the pristine GO film such as hybridized carbon atoms (SP<sup>3</sup>) and carboxyl's (O–C = O). Accordingly, the electrical conductivity increases from 0.11 S/m of pristine GO to an optimum value of 0.46 S/m after 5 min of plasma treatment, as a result of the incorporation of high amount of carboxyl, hydroxyl and carbonyl groups. The current results indicate that the properties of GO can be tuned by varying the degree of oxidation, which may pave the way for new developments in GO-based applications.

Address correspondence to E-mail: m.abdelhamid999@gmail.com

## 1 Introduction

Carbon-based materials in a 2D crystal lattice form such as graphene and its derivatives like graphene oxide (GO) and reduced graphene oxide (rGO) were first reported in 2004 [1]. They exhibit unique electrical and electronic properties that hold highly promising potential for the up and coming generation of various optoelectronic devices, energy conversion, and sensors [2, 3]. These applications resulting from its exceptionally low sheet film resistance, thermal conductivity, high optical transmittance, and great mechanical stability [4].

Graphene oxide (GO) is a form of graphene functionalization. GO has unique advantages such as easy functionalization, solution processability, mass production, and low cost; as a result, it is an attractive nanomaterial [5, 6]. GO material has oxygen interceded carbon network, large work function (WF) and insulating properties, which is valuable for conductive electrode applications, such as solar cells [7], touch screens [8], organic optoelectronic devices [9], and hole transport in organic electronic devices [10, 11]. The adjusted Hummer's strategy is one of the most widely utilized methodologies for synthesizing GO films [12]. Strong oxidizing agents are utilized to change over the graphite to GO, through regularly covalently functionalized with hydroxyl, epoxy, carbonyl, and carboxyl groups, which is required in many electronic applications [13, 14].

The oxidation level of GO is thusly constrained by different reductants like hydroiodic acid, L-ascorbic acid, sodium borohydride and hydrazine [15]. In particular, GO is effectively dispersed in the solvent and utilized in solution-processed organic photonic devices due to oxygen containing functional group [16]. The GO improvement to support GO-based applications needs a specific control over its surface covalent functionalization. Therefore, the GO surface is considered as an influencing environmental compatibility factor.

Generally, there are various methods of surface treatment processes. Among these, RF plasma surface treatment stands as a highly appreciated technique. It is generated using a high RF electric field (normally 13.56 MHz) and mainly characterized by a low-temperature plasma. Previously, RF plasma surface treatment was applied to improve the mechanical and electrical performance of various materials [17]. In this process, the materials surface properties can

be modified through reacting with active plasma species and radiations including electrons, ions, radicals, and ultraviolet radiation [18]. Plasma surface treatment of GO films leads to the creation of crystalline defects or separate chemical bonds on film surface, which in turn improves its surface functionalization [19, 20].

The cold RF plasma is an effective, eco-accommodating, and low-cost technique that provides the GO film with high quality surface properties and good chemical nature; leading to an enhancement of the functionalization and reduction features of GO [19]. Mostly, GO is functionalized by plasma treatment in the presence of nitrogen, ammonia, oxygen, methane, hydrogen, and fluorine. The oxygen plasma treatment is one of the effective techniques that widely utilized for enriching the GO films with oxygen functional groups. Accordingly, the chemical and physical properties of GO films can be changed and let the modified films to be more interesting for various hydrophilic-based applications [21–24]. Moreover, the oxygen plasma significantly reduces the degree of disorder of graphene lattice defects leading to high changes in structural properties and partial reduction of GO, forming a reduced graphene oxide (rGO) [25]. Besides, the GO films can be reduced chemically [26], thermally [27, 28], or by an ultraviolet-assisted method [29], and the obtained rGO semiconductor has higher electrical conductivity than GO material. Furthermore after oxygen plasma treatment, the charge transport properties of GO as a hole transport layer (HTL) have been improved by modifying the C-O chemical bonds [30, 31].

Although plasma surface treatment was previously used to modify the surface of carbon-based materials, the use of RF oxygen plasma technique is still limited. The main objective of this research work is to improve the electronic performance of GO films for solar cells and other electronic/optoelectronic applications. RF plasma oxidation with treatment temperature lower than 100 °C has used to change the chemical nature of the GO layer through the creation of new functional groups. Further, the reduction level of the GO layer is expected to be modified after treatment. In order to achieve a complete study, the microstructural, electrical, optical, and morphological properties of the plasma-treated GO films compared to that of the pristine one were examined and discussed.

## 2 Experimental procedures

### 2.1 Synthesis of GO nanoparticles (NPs)

Table 1 shows the materials used in the GO preparation process. Graphite powder was oxidized via the modified Hummer's method to form graphite oxide as seen in Fig. 1. Briefly, three grams of graphite precursor are increasingly added to 320 ml of  $\text{H}_2\text{SO}_4$  solution (98% concentration) in a flask, which placed in magnetic stirrer. Subsequently, 80 ml of  $\text{H}_3\text{PO}_4$  solution is dropwise slowly in the flask under stirring. The resulted mixture is continuously stirred for 2 h, while 18 g of  $\text{KMnO}_4$  powder is slowly added to the mixture to prevent the rapid rise in temperature. An important requirement for completing the oxidation process is the presence of a strong oxidizing agent ( $\text{KMnO}_4$ ) and a strongly acidic medium while maintaining a low temperature (not exceed 40 °C) throughout the experiment to avoid the reduction process. In order to oxidize the graphite, the one-pot mixture was left for stirring for 72 h. As a result, the solution color is observed to be changed from black to dark green. Subsequently, at room temperature (RT), the  $\text{H}_2\text{O}_2$  solution was supplementary added to break the oxidation process and remove the  $\text{KMnO}_4$ . The color of the resultant suspension is bright yellow indicating a high level of oxidation graphite process [32, 33]. To remove any remaining acid, the formed GO is washed three times with 1 Molar of HCl aqueous solution [34], hence, washed repeatedly with distilled water until a pH range 6–7 is achieved. Finally, the obtained solution dried at an elevated temperature of 50 °C for 3 h to get graphene oxide powder.

### 2.2 Synthesis of GO films

In the beginning, the glass substrates are cleaned by a dilute acidic solution of HCl. Then, they are extensively rinsed with distilled water to remove the

residual HCl. After that, the glass substrates are sonicated in acetone to remove the organic impurities and lastly rinsed with deionized water. Hence, the obtained GO powder is dissolved in distilled water solution. The resultant suspension is deposited on the glass substrates by a spin coating process using 1000 rpm for 30 s. Finally, the formed films are dried at an elevated temperature of 50 °C for 1 h.

### 2.3 Plasma surface treatment of GO films

Surface treatment with oxygen and applying an inductively coupled plasma (ICP) has been used to enhance the physical and chemical properties of the obtained GO films. Figure 2 displays the schematic diagram of the ICP system with a matching network circuit. It comprises of a quartz reactor tube of 50 cm in length and 4.15 cm in diameter. The film substrate is mounted on a water-cooled copper sample holder of 3.6 cm in diameter. Prior to letting gas in, the air within the reactor tube is pumped out by a rotary pump to a base pressure of  $2 \times 10^{-6}$  bar. The pressure is measured using a Pirani gauge. A channel controlled by a mechanical needle valve is used to introduce the oxygen gas into the reactor tube up to a working pressure of  $1 \times 10^{-4}$  bar. The oxygen plasma discharge is generated by a water-cooled copper induction coil energized by a 13.56 MHz RF power supply model HFS 2500 D via a tunable matching network as shown in Fig. 2. The as-prepared GO films are exposed to the oxygen plasma discharge at a processing power of 100 W for different processing times of 1, 3, 5, and 7 min. Normally, we treat the samples in this reactor at a distance of approx. 3 cm between the middle of plasma and the sample surface. However, for the current samples, the distance between the plasma and the film surface is increased to 7 cm to ensure that the film surface is to preserved at low temperatures during the plasma treatment. A Chromel–Alumel thermocouple is attached to the surface of the GO films to measure the treatment

**Table 1** Materials used in the GO preparation process; all chemical materials were purchased from Sigma Aldrich

Materials	Sulfuric Acid	Phosphoric Acid	Graphite Precursor	Potassium Permanganate	Hydrogen Peroxide	Hydrochloric Acid	Distilled water
Chemical formula	$\text{H}_2\text{SO}_4$	$\text{H}_3\text{PO}_4$	–	$\text{KMnO}_4$ , 99%	$\text{H}_2\text{O}_2$ , 30%	HCl, 37%	–

**Fig. 1** Schematic flow chart of Hummer's modified method of GO powder formation, spin coating technology for depositing GO films

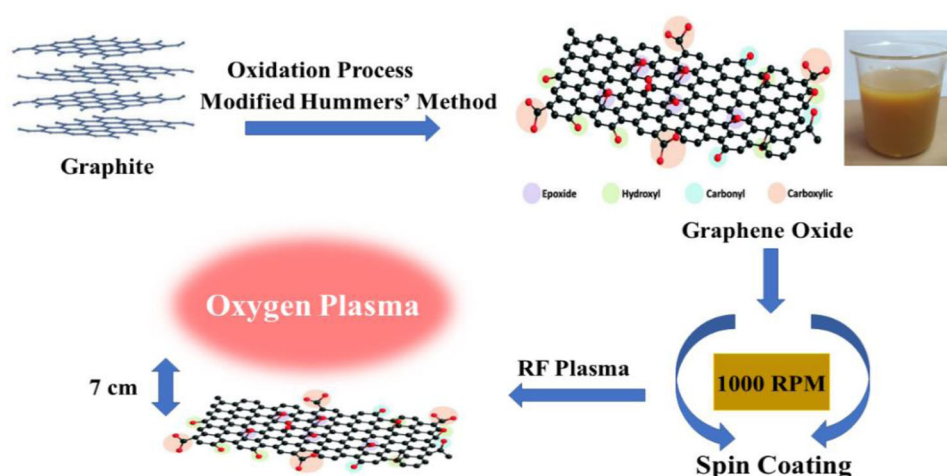
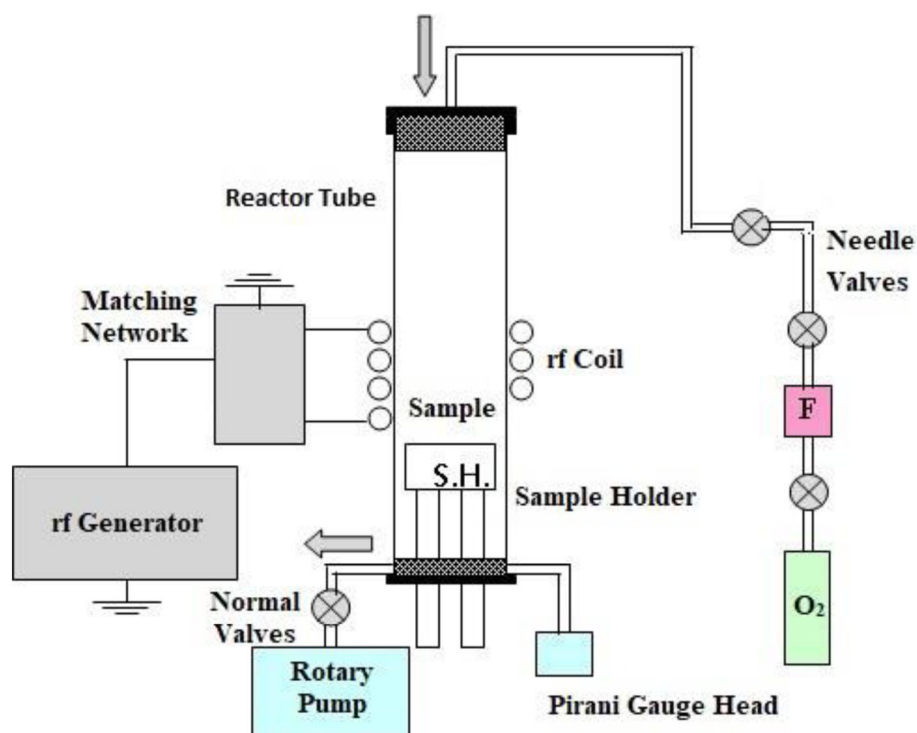


**Fig. 2** The GO plasma oxidation system powered by RF discharge



temperature during the plasma modification process. The plasma runtime increases the GO surface temperature from 52 °C to 81 °C. After completion of plasma treatment, the treated sample is allowed to cool inside the evacuated reactor tube to room temperature before removing it from the tube.

### 3 Characterization techniques

X-ray photoelectron spectroscopy (XPS) is employed to examine the chemical compositions of the GO films. XPS data was collected on a Thermo Fisher Scientific K-ALPHA X-ray photoelectron spectrometer with a monochromatic X-ray Al K $\alpha$  radiation energy as an excitation source is 1486.6 eV, 400  $\mu$ m spot size, 200 eV full spectrum pass energy, and 50 eV narrow-spectrum. Moreover, detection of adventitious carbon on the sample surface is not considered. As usual, GO is prepared in the lab and mostly

composed of the  $sp^2$  group, while the  $sp^3$  group was sensed after chemical oxidation. So, the detection of contaminated carbon can be considered as adventitious carbon layers on the metal surfaces before and during the sample preparation or by maintaining the samples in an insufficiently evacuated environment. To maintain an accurate XPS examination, the spectra were carefully referenced to the  $sp^2$  and  $sp^3$  graphitic carbon C1s line energy, which was set at  $285 \pm 0.1$  eV binding energy. A rigorous method for fitting the complex peaks was applied here thus providing more accurate position determinations, i.e. the chemical shift, as well as the integrated intensity of the component peaks representing the various bonding states. A Gaussian–Lorentzian peak form (G/L ratio 70/30) was used for the peak decomposition of O1s and for the reacted C1s lines in this work according to our instrument environment. Raman spectroscopy has been used to characterize the chemical composition and structure of the samples. Raman spectra were collected using a dispersive Raman microscope SENTERRA (Bruker, Germany) equipped with a laser source of 532 nm wavelength. Besides, the thermal stability of the GO films was studied by a simultaneous DSC/TGA model SDT Q600 (USA). The thermogravimetric analysis (TGA) was operated with nitrogen ( $N_2$ ) gas at RT and up to 500 °C with a ramp rate of 10 °C/min. The surface morphology of all the GO sheets was analyzed using a high-resolution transmission electron microscope (HR-TEM, JEOL JEM-2100) (Japan). The contact angle, wet energy, surface tension, diffusion of power factor, and the adhesion force were measured using a contact angle analyzer (SEO Phoenix 300). Moreover, a profilometer (Talysurf 50-Taylor Hopson precision) was used to measure the surface roughness (Ra) of the GO films. Furthermore, the four-point probe method has been used to evaluate the electrical resistivity using an EQ-JX2008-LD resistivity tester. The average electrical resistivity of each film was calculated from at least 10 readings gained from various parts. All solutions and suspensions were coated on the glass substrates using a spin coater machine (SpinNXG-P1).

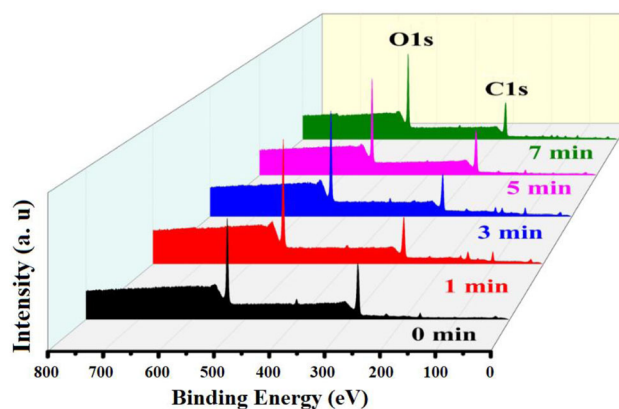
## 4 Results and discussion

### 4.1 X-ray photoelectron spectroscopy (XPS)

XPS is used to obtain insights into changes in the surface chemical composition of GO films treated with oxygen plasma using different processing times compared to pristine GO film. XPS analysis are shown in Fig. 3. A predominant graphitic C1s peak ca. 285 eV and an O1s peak at ca. 532 eV are observed in the XPS survey spectra of all films.

The XPS atomic concentration of C and O for the pristine and treated GO films has been calculated and shown in Table 2. It is calculated from the ratio between the area of C1s peak and the area of O1s peak. Then, a fitting process is applied on the data to quantitate the C and O ratios in each sample.

Figure 4 shows the deconvoluted C1s and O1s of the pristine and treated GO films. The fitting data of C1s and O1s XPS spectra is helpful to accurately track the evolution of carbon and oxygen groups of the pristine GO film and the treated GO films at different processing times. The curve deconvolution of the C1s peak shows five peaks designated as C1 (C = C/C–C in aromatic, 284.7 eV), C2 ( $sp^3$  hybridized carbon atoms and hydroxyls (C–OH), 285.7–285.3 eV), C3 (epoxides (C–O–C), 286.8 eV), C4 (carbonyls (C = O), 287.4 eV) and C5 (carboxyl's groups (O–C = O), 288.4 eV) [35–38]. The O1s spectrum can be divided into O1 (532.6–531.3 eV), O2 (532.7 eV), and O3 (535 eV), which is assigned to C = O, C–O, and adsorbed  $H_2O$ , respectively [39, 40]. With this in mind, current plasma experiments are worked at limited temperatures in the range of 52–81 °C. For the deconvoluted C1s spectra shown in Fig. 4, the bonds of C–C, C = C

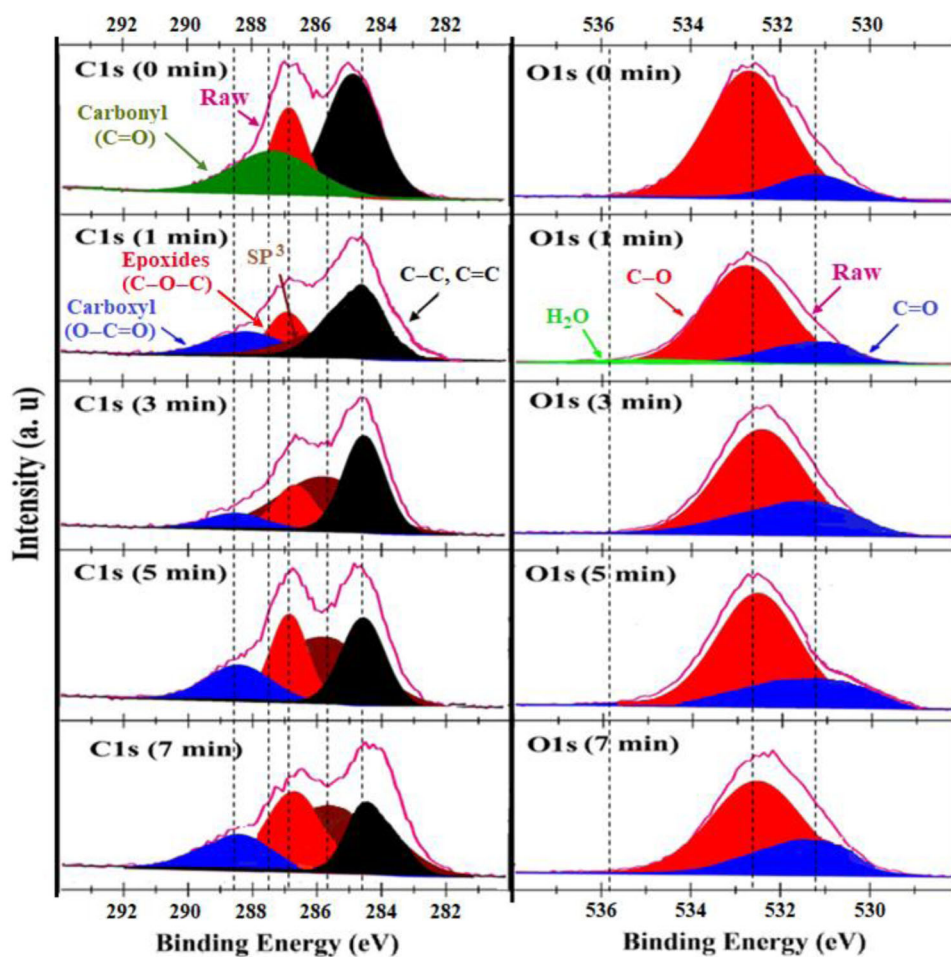


**Fig. 3** The XPS survey of pristine and plasma treated GO films



**Table 2** Fitted results (at. %) of C1s and O1s XPS spectra of the pristine and plasma treated GO films

O1s (%)			C1s (%)					Binding energy (eV)
O3 (535)	O2 (532.7)	O1 (532.6–531.3)	C5 (288.4)	C4 (287.4)	C3 (286.8)	C2 (285.7–285.3)	C1 (284.7)	
H <sub>2</sub> O	O–C	C = O	Carboxyl's (O–C = O)	Carbonyls (C = O)	Epoxides (C–O–C)	Hybridized Carbon atoms (SP <sup>3</sup> )	Aromatic C–C, C = C	
–	84.00	16.00	–	26.10	22.70	–	51.19	0 min
5.23	78.50	17.30	15.51	–	15.33	30.23	38.93	1 min
–	76.39	23.61	7.03	–	15.12	42.70	35.09	3 min
–	79.36	20.46	15.11	–	30.70	27.52	26.67	5 min
–	72.59	27.41	12.12	–	21.60	42.21	24.07	7 min

**Fig. 4** Deconvoluted C1s and O1s of the pristine and plasma treated GO films

and epoxides (C–O–C) groups are presented in a high quantity in the pristine GO film (0 min). However, the pristine GO films are gradually reduced after exposing to oxygen plasma treatment at different processing times of 1, 3, 5 and 7 min. Plasma surface

treatment leads to disappear the carbonyls groups (C = O) and creates new chemical bonds of hybridized carbon atoms (SP<sup>3</sup>) and little amount of carboxyls (O–C = O). Further, Fig. 4 illustrates the deconvoluted spectra of O1s. The observed

functional groups such as C = C, C–C, and H<sub>2</sub>O are highly affected after plasma treatment. It leads to the removal of most of the thermally unstable oxygen components in the graphene. This is supposed to be in correspondence with previous work [41]. The O1 peak is attributed to singly-bonded oxygen in alcohols. Epoxies, esters and the hydroxyl groups are mainly resulted from water adsorption on graphene. The O2 peak is associated with carbonates, while the O3 peak corresponds to hydroxides [35].

Figure 5 presents the oxygen amount in oxygen-containing groups of (C–O–C), (C = O), and (O–C = O) derived from C1s spectra of the pristine and treated GO films at different processing times of 0, 1, 3, 5 and 7 min. The oxygen amount is decreased from its maximum value (48.8 at.%) in oxygen-containing groups of the pristine GO film to a minimum value of 22.15 at.% after plasma treatment at the processing time of 3 min. This is mostly attributed to that the rate of oxygen release is greater than the oxygen insertion rate during oxygen plasma treatment. However, at relatively longer plasma processing times, the amount of oxygen is gradually increased and reaches up to 42.82 at.% at the processing time of 5 min. This can be ascribed to the relative increase in the oxygen insertion rate. By observing the data in Table 2 and Fig. 5, this variation in oxygen amount insures a partial reduction in GO films after plasma treatment. It is followed by a disappearance of carbonyls (C = O) group and an effective change in the chemical composition of other functional groups. Further, a new functional group of (O–C = O) is created

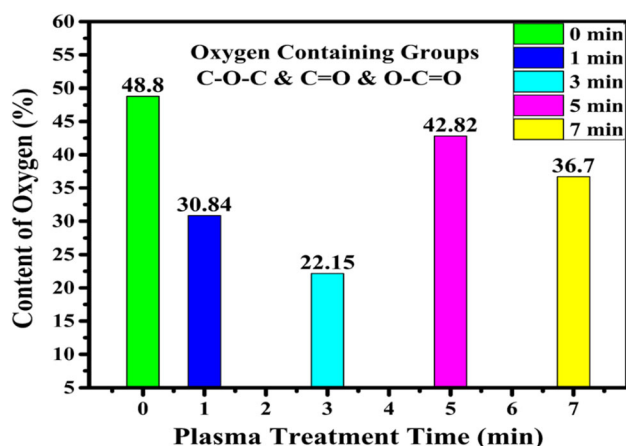


**Fig. 5** Amount of oxygen-containing groups (C–O–C), (C = O), and (O–C = O) derived from C1s spectra of the pristine and plasma treated GO films at different times of 0, 1, 3, 5 and 7 min

beside the formation of the hybridized carbon atoms (SP<sup>3</sup>). The change in chemical composition and characterization in the treated GO films leads to significantly affect their physical and chemical properties [42, 43].

## 4.2 Raman spectroscopy

Raman spectra were employed to characterize the effect of oxygen plasma treatment on the structural features of GO films. Whereas, it is possible that the chemical oxidation process induces structural changes in the graphite lattice thanks to the growth of various forms of oxygenated function groups at the basal plane as well as at the edges. Raman spectroscopy, as a non-destructive method, is the standard tool for assessing the defective properties of the GO sheet structure [38]. The D-band is recognized to the first-order Raman scattering of A<sub>1g</sub> and breathing mode of the aromatic rings; it requires a defect for activation. It is only detected at defect sites in the grapheme-based lattice materials. Whereas the G-band is a result of the doubly degenerate zone breathing center E<sub>2g</sub> mode [44]. As shown in Fig. 6a, the D-band at around 1342 cm<sup>-1</sup> is assigned to the defects on graphene sheets, while the G-band observed at around 1586 cm<sup>-1</sup> is assigned to the in-plane vibration mode of sp<sup>2</sup> carbon atoms. In addition, the full width half maximum (FWHM) of the G band increases in relation to the oxidation level. As estimated, the FWHM of the G-band was found to be 51, 68, 72, 73 and 69 cm<sup>-1</sup>, with less defective structures of the treated samples at 0, 1, 3, 5 and 7 min, respectively. The gradual increase in the FWHM values is mostly attributed to the changes in the oxidation levels which indicates an increase in the sp<sup>3</sup> carbons. Along these lines, to qualitatively investigate the level of film defect, the Raman I<sub>D</sub>/I<sub>G</sub> intensity ratio can be used [45]. Some previous works have shown that the defect level (I<sub>D</sub>/I<sub>G</sub> ratio) of the GO films has been improved after the plasma treatment [46–48]. Figure 6b revealed that the I<sub>D</sub>/I<sub>G</sub> ratio decreased after the plasma treatment compared to the pristine GO film, which is less than the known value of the I<sub>D</sub>/I<sub>G</sub> ratio for GO (~ 1). Herein, increasing the processing time leads to a relative increase in the I<sub>D</sub>/I<sub>G</sub> ratio. This increase is attributed to the formation of new defects and disordered carbon or amorphous carbon on the GO surface due to the deposition of carbon-based species from plasma (in agreement

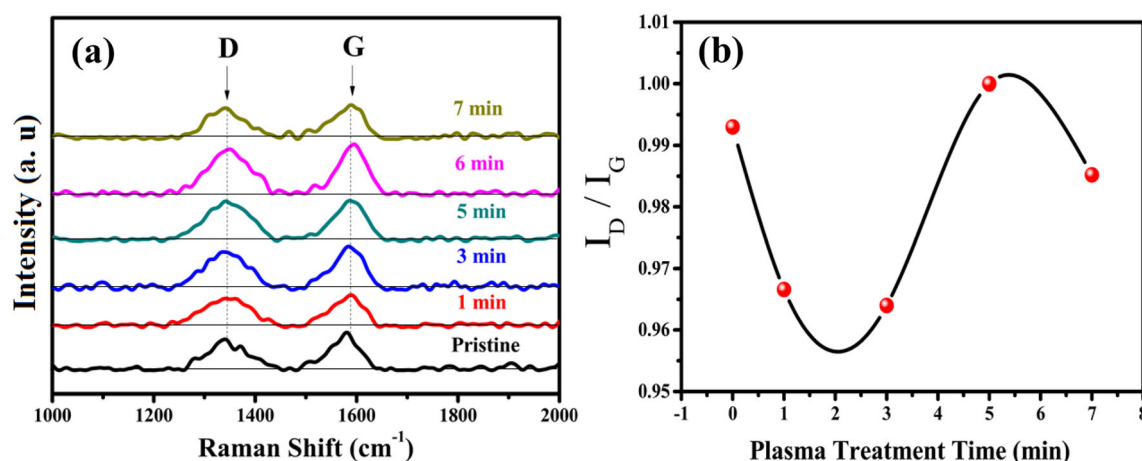


**Fig. 6** a Raman spectra of the pristine GO and the plasma treated GO films, b  $I_D/I_G$  ratio versus the treatment time

with the XPS data) [46, 47, 49]. The reduction of functional groups, defect level, and the in-plane  $sp^2$  crystallite size can be determined by the relative intensity of D and G-band peaks ( $I_D/I_G$ ) [44, 50].

Moreover, the FWHM of the D-band is frequently considered a measure of surface defect sites. The FWHM of D-band increased from  $86.7\text{ cm}^{-1}$  for the pristine GO to  $100.3\text{ cm}^{-1}$  for the plasma treated film for 5 min, indicating a more defective structure for the latter. However, it decreased to  $81.4\text{ cm}^{-1}$  after 7 min in the atmosphere of oxygen plasma, suggesting a small fraction of defects generated within treated GO films [12].

### 4.3 Thermogravimetric analysis (TGA)

The thermal stability and surface functionalization degree of the pristine and treated GO samples were investigated by TGA analysis. Figure 7 displays the

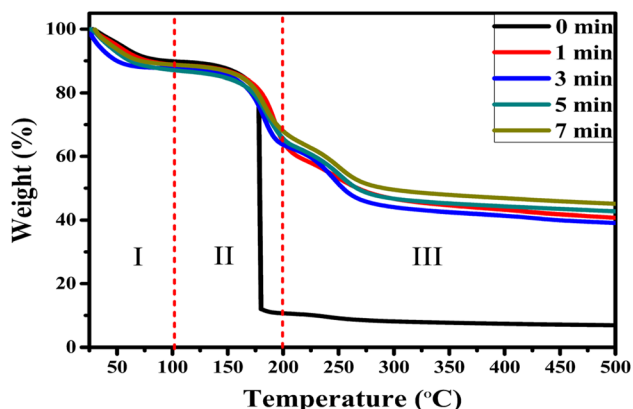


**Fig. 7** TGA curves of the pristine and plasma treated GO samples under nitrogen atmosphere

TGA curves that present the material weight loss as a function of temperature under nitrogen atmosphere, while Table 3 presents the percentage of weight loss at different temperature ranges. As shown in Fig. 7, three regions (I, II, and III) can be distinguished in the TGA spectra of the pristine and plasma treated GO films. The first region I (up to  $100^\circ\text{C}$ ) shows the evaporation of the absorbed water molecules which leads resulting in a decrease in the water content in the GO films (high hydrophilicity) [35]; causing a weight loss of more than 10%, as shown in Table 3. In the region II ( $100\text{--}200^\circ\text{C}$ ), the pyrolysis and functional groups of affixed oxygen (such as carboxyl, epoxy, lactone) were decomposed producing  $\text{CO}$ ,  $\text{CO}_2$  and  $\text{H}_2\text{O}$  vapor [49, 51]. In this temperature range, the pristine GO film shows a maximum weight loss close to 80% at about  $180^\circ\text{C}$ , which indicates that the pristine GO shows a high pyrolysis decomposition of labile oxygen functional groups such as those of hydroxyl and epoxy [52]. After only 1 min of oxygen plasma treatment, the weight loss of the treated GO film increases to 19.92%; indicating a further reduction in the GO film. The weight loss

**Table 3** Weight losses of the pristine and plasma treated GO films

Temperature ( $^\circ\text{C}$ )	Weight loss (%)				
	0 min	1 min	3 min	5 min	7 min
30–100	10.12	11.44	12.57	13.35	11.34
100–200	80.07	19.92	23.91	21.09	20.86
200–500	83.02	27.94	24.52	22.92	22.75
30–500	93.13	59.30	60.99	57.36	54.96



increased to about 23.91% at processing time of 3 min, and it was measured to be around 21% for films processed at higher plasma times. This leads to a partial reduction in the treated GO films and additional changes in the chemical characterization which generates small defects and forms new chemical bonds as shown in XPS and Raman analysis.

At a higher temperature range of 200–500 °C (region III), the most stable groups like carbonyl and aromatic (quinone) are mostly decomposed due to the pyrolysis of the carbon skeleton [51]. As observed, the pristine GO film has a maximum weight loss of 83%. After just 1 min of oxygen plasma treatment, the weight loss is sharply increased to 27.94%. Then, it is gradually decreased to 22.75% by increasing the processing time up to 7 min. Therefore, it can be concluded that the pristine GO contains more carbonyl/quinone groups than the plasma treated GO films, which is in good agreement with XPS results. Finally, the temperature range of 30–500 °C shows a higher value of total weight loss for the pristine GO sample compared to that of all plasma treated GO samples (Table 3).

The thermal decomposition of GO material is largely consistent with the values measured in the current TGA analysis [49, 53]. Furthermore, it supports the creation of new oxygen-containing groups as well as different proportions from the original groups existed in the pristine GO film. Accordingly, the thermal stability of GO materials is maintained. The differences in the features of TGA curves and weight loss of GO samples emphasized the formation of various types of functional groups during the oxygen plasma treatment. These results, in addition to the Raman results, confirm that cold RF oxygen plasma can be used for functionalization of GO.

#### 4.4 Morphological characterization

A high-resolution electron transmission microscope (HR-TEM) was used to investigate the nature of GO treated with various degrees of oxidation, using plasma at power of 100 W for different processing times, in the surface morphology, as shown in Fig. 8. As seen in Fig. 8a, the stacked multilayers of the as prepared GO film led to the surface being identified as a semitransparent sheet with minor surface defects like morphology. For samples treated at 1 and 3 min, Fig. 8b,c reveals a sheet like leaf morphology of a multilayer structure consisting of partially oxidized

GO films. As illustrated, the GO sheet is observed with a reduced layer number. Moreover, as the time of plasma treatment increases, the film transparency rapidly improves. Increased transparency is due to the formation in the oxidation process of functional groups including hybridized atoms of  $sp^3$ . A similar effect was previously detected for GO sheets after oxygen plasma treatment [54]. The processing effect can be mainly concentrated on the removal of epoxides, carbonyls and carboxyl groups of instable oxygen atoms and a number of functional oxygenated groups from the interplanar of GO sheets [54]. Figure 8d,e presents the GO surface after relatively longer treatment time of 5–7 min. The treated surface has lower dimensions and higher transparency compared to that of the less oxidized samples (1–3 min). Increases in the highly oxygenated functional groups with new defects and disordered or amorphous carbon in the treated sheets have resulted in a high transparency effect, in line with the Raman findings. The disordered and unwrinkled structure during the plasma process was attributed to the increase in treatment temperature or to an increase in the amount of oxidant plasma species [55]. Finally, it is reasonable to conclude that the morphology, dimensions, and transparency of the GO sheets are highly dependent on the degree of oxidation and the effect of plasma etching.

#### 4.5 Contact angle

The GO material is usually exhibiting hydrophilic property, which is very important for electrical applications [56, 57]. This hydrophilic property arises from the hydroxide and was found to be improved after the oxygen plasma treatment [58]. The immersion of pristine film surface in a medium of low-temperature oxygen plasma containing various plasma species are responsible for generating many chemical reactions in the graphene flakes. This process provides  $sp^3$  hybridization and leads to the formation of a C–OH bond that enhances the hydrophilic properties. The improvement in the GO hydrophilic features is mostly due to the effect of generating new hydrogen bonds [58, 59].

After plasma treatment of GO films, contact angle (CA) measurements utilized to investigate the degree of hydrophilicity. The pristine GO film has a contact angle of 50.45°. The contact angles of the plasma treated GO films increased from 55.46° to 61.31° by

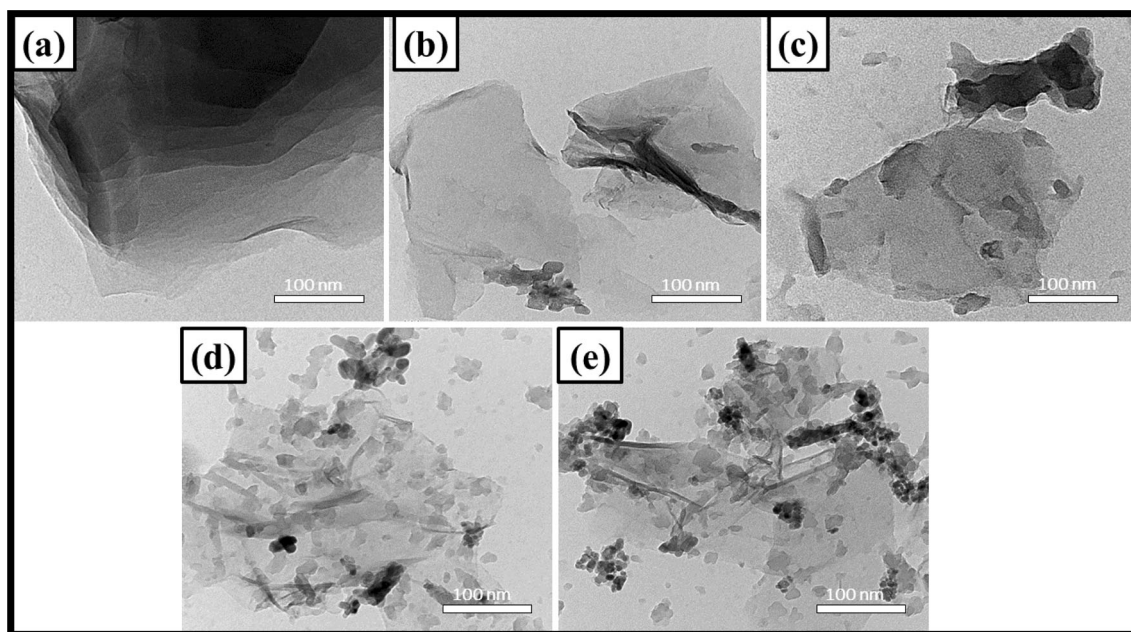


**Fig. 8** HR-TEM images of GO with different degrees of oxidation for plasma power of 100 W at various processing times **a** 0 min, **b** 1 min, **c** 3 min, **d** 5 min and **e** 7 min

increasing the treatment time from 1 to 3 min, then it decreased to about  $47.87^\circ$  at a processing time of 5 min as shown in Fig. 9. This improvement in the

hydrophilicity is attributed to the unusual chemical reactions between the GO and the oxygen plasma species that creates vacancies or sites of C–H,  $SP^3$  or

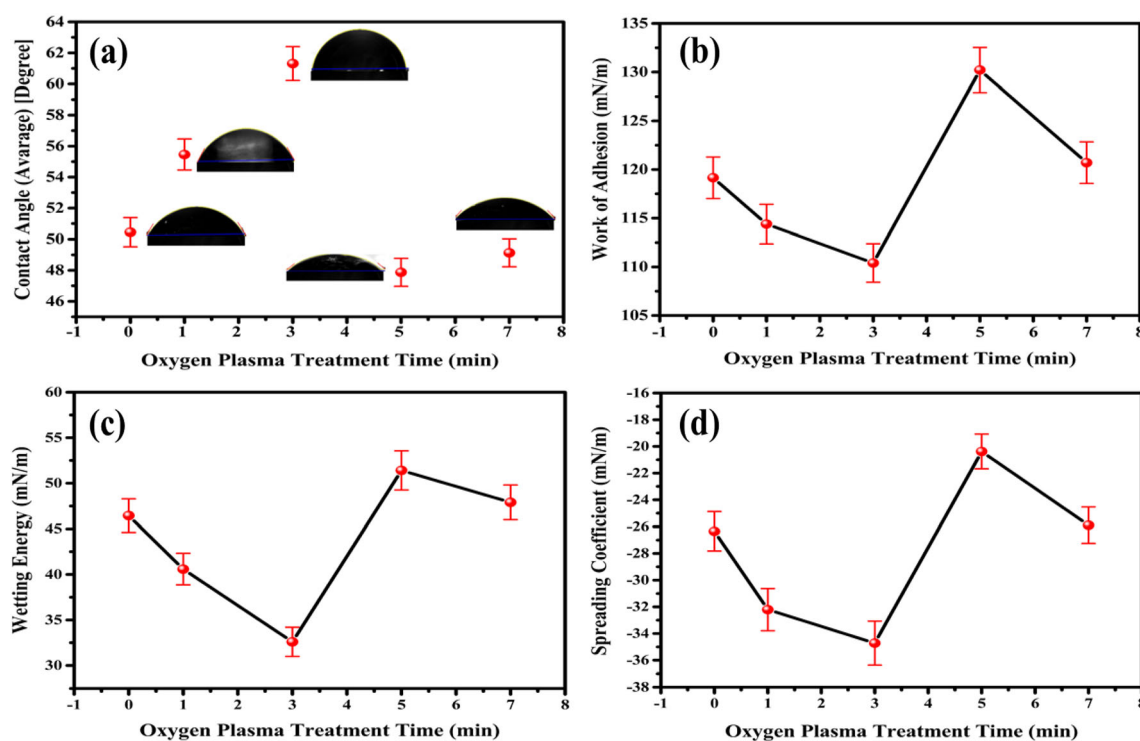


**Fig. 9** **a** Contact angle, **b** work of adhesion, **c** wetting energy, and **d** spreading coefficient curves of the pristine and treated GO films at various treatment times

OH-bond, causing damage and defects within the graphene flakes [59]. This noticeable property of hydrophilicity can be ascribed to the convergence of water molecules with the oxygenated functionalities presented into the surface of the GO with increased processing time [60].

The work of adhesion is determined by knowing the adhesion force between the GO film and droplet water which it can be calculated from the next equation, Eq. (1) [61].

$$W_{sl} = \gamma_s + \gamma_l + \gamma_{sl} \quad (1)$$

where  $\gamma_s$  is the solid surface free energy while  $\gamma_l$  refers to liquid (water) surface free energy, and  $\gamma_{sl}$  denotes solid–liquid interfacial energy.

Combining this equation with the Young–Dupré equation, Eq. (2):

$$\gamma_s = \gamma_{sl} + \gamma_l \cos \theta_e \quad (2)$$

gives the next equation, Eq. (3) [62]:

$$W_{sl} = \gamma_l (1 + \cos \theta_e) \quad (3)$$

where  $\theta_e$  stand for the equilibrium (Young's) contact angle between the plasma treated GO film and water, while  $\gamma_l$  symbolizes the surface tension of water on the solid surface. The adhesion work of the GO films decreased from 119.15 to 110.4 mN/m by increasing the processing time from 0 to 3 min, while the optimum value of 130.4 mN/m was obtained after 5 min of plasma treatment.

Moreover, the oxygen plasma treatment affects the chemical and physical features of the GO films and in turn, it has a great effect on the hydrophilic spices on surface properties of the GO films leading to enhance their wettability and spreading coefficient [63–66]. As previously found the arrangement of more hydrogen bonds between the water drops and GO films increases the molecular dipole/dipole interaction, which in turn improves the wettability [67–69]. The optimum values of wettability (27.41 mN/m) and spreading coefficient (– 45.38 mN/m) are achieved after 5 min of oxygen plasma treatment.

#### 4.6 Roughness measurements

The plasma environment contains fast electrons, ions, and neutral species that bombard the sample surface affecting its surface roughness. Herein, the surface plasma treatment of GO films at different processing times leads to wrinkles and roughness variations on

the GO surface. These indicate that the graphene removal by the oxygen plasma process is almost like an anisotropic vertical etching, changing the properties of the graphene surface [70]. This hypothesis is supported by measuring of surface roughness factors like average roughness (Ra) and root mean surface roughness (Rq) which presented in Fig. 10. The values of Ra and Rq reduced from 7.8 and 9.6  $\mu\text{m}$  for the pristine sample to 6.6 and 8.6  $\mu\text{m}$  after 3 min oxygen plasma treatment. However, by increasing the processing time to 5 min, the roughness parameters are increased to the optimum value (Ra = 8.7  $\mu\text{m}$  and Rq = 11.3  $\mu\text{m}$ ). These results attributed to the contribution of low-temperature oxygen plasma treatment to chemical reactions on the GO surface that increased the defect density, grain refinement, and the amount of C–O–C epoxides functional groups during the plasma process [58]. Therefore, agglomeration can occur on the surface after treatment, which affects the surface roughness [58]. The production of wrinkles on the treated GO film surface during the cooling process is caused by a surface heat shrinkage [42]. Moreover, it is known that, the heat shrinkage has an effect on the strength of Van der Waals between the GO and the substrate, which is responsible for the film adhesion to the substrate [70, 71]. Plasma surface treatment may cause some wrinkle structures which increase the film adhesion.

#### 4.7 Electrical properties

Figure 11 shows the film resistance and electrical conductivity of the pristine GO film and the treated GO films at different plasma processing times. The

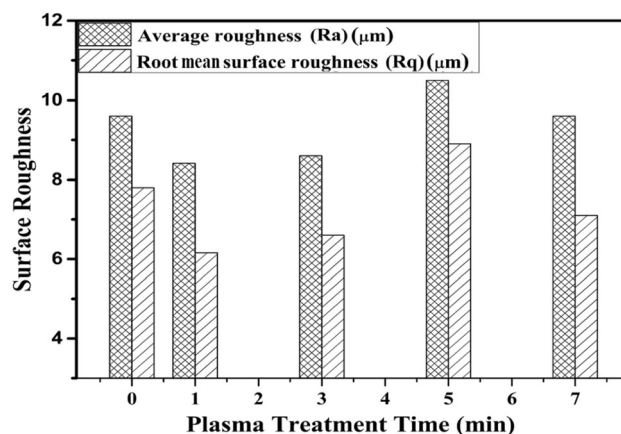


**Fig. 10** Surface roughness parameters for the pristine and the treated GO films at various plasma processing times

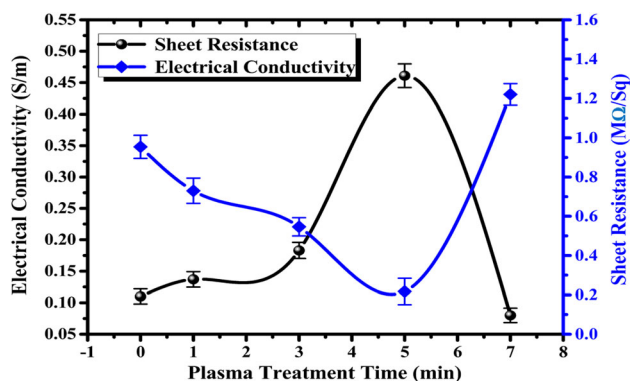


**Fig. 11** Film resistance and electrical conductivity behavior of the GO films before and after plasma treatment at various processing times

current measurements confirmed/approved that the oxygen plasma treatment has a significant effect on the electrical resistance and conductivity of the obtained films. The measured resistivity value of the pristine sample is 0.95 MΩ/square and it is gradually decreased to reach 0.22 MΩ/square by increasing the plasma processing time to 5 min. Accordingly, the electrical conductivity increased by increasing the processing time from 0.11 S/m for the pristine sample to an optimum value of 0.46 S/m after 5 min treatment. As previously shown in literature the oxygen plasma treatment has been used to improve the electrical conductivity of the GO and rGO [49, 70, 72]. The current results are consistent with the fact that, the use of oxygen plasma as gaseous precursors on the carbon surface allows an improvement in the amount of carboxyl, hydroxyl and carbonyl groups, which in turn affect the electrical response of the materials [72]. The treated sample at a processing time of 7 min showed an inconsistency with this behavior; giving an increase in film resistance to 1.22 MΩ/square and a decrease in the electrical conductivity to 0.082 S/m. According to the XPS and TGA results, the plasma-treated GO films at 1, 3 and 5 min contained a higher amount of (O–C = O) carboxyl's and SP<sup>3</sup> groups of carbon atoms compared to GO films treated with plasma 7 min. Carbonyl/ quinone can facilitate the reactions of oxidation and reduction [50, 73, 74]. Moreover, the oxygen plasma etching is normally used on the graphene to induce the semiconductor properties. Further, the ohmic contact property in graphene is not destroyed after oxygen plasma treatment. The decrease in electrical

conductivity in the sample treated at 7 min might be attributed to the etching effect [70].

## 5 Conclusion

Pristine and modified GO films using oxygen plasma treatment, for processing power of 100 W, were successfully synthesized and characterized as potential candidates for many electronic applications. The oxygen plasma process has demonstrated a great enhancement in both the physical and chemical properties of GO films by influencing their chemical composition. XPS demonstrated the removal of a high amount of oxygen-containing groups such as epoxides, carbonates, and carboxyl groups. As a result, the oxygen-containing groups decreased from 48.8 at.% for pristine to 36.15 at.% for the treated GO for 5 min. However, at relatively longer plasma processing times, the oxygen amount is gradually increased and reached up to 41 at.% at the processing time of 7 min. Moreover, the results of Raman spectroscopy and TGA revealed the introduction of large amount of oxygen groups after increasing the oxygen plasma treatment times and maintaining the thermal stability of the materials (38.17 at.% difference in weight loss between the pristine GO and the treated GO at 7 min). The HR-TEM surface morphology for all samples showed a sheet like structure with various transparency. The treatment at different plasma processing times leading to wrinkles and roughness variations on the GO surface, where Ra decreased by increasing the treatment times up to 5 min. Furthermore, the contact angle increased from 55.46° to 67.87° by increasing the treatment time from 1 to 5 min. The property of hydrophilicity attributed to the convergence of water molecules with the oxygenated functionalities presented into the surface of the GO as the processing time increases. Finally, the electrical conductivity increased from 0.11 S/m to the optimum value 0.46 S/m at treatment time 5 min that attributed to the incorporation of a high amount of carboxyl, hydroxyl, and carbonyl groups during plasma process, which in turn affected the electrical response of the GO materials. This study gives good results for solar cell applications.



## References

1. K.S. Novoselov, A.K. Geim, S.V. Morozov, D. Jiang, Y. Zhang, S.V. Dubonos, I.V. Grigorieva, A.A. Firsov, *Science* **80**, 306 (2004)
2. X. Jiang, R. Zhang, T. Yang, S. Lin, Q. Chen, Z. Zhen, D. Xie, H. Zhu, *Surf. Coatings Technol.* **299**, 22–28 (2016)
3. S.K. Vashist, J.H.T. Luong, *Carbon N. Y.* **84**, 519–550 (2015)
4. S. Chen, W. Cai, R.D. Piner, J.W. Suk, Y. Wu, Y. Ren, J. Kang, R.S. Ruoff, *Nano Lett.* **11**, 3519–3525 (2011)
5. M.E. Azim Araghi, E. Omman, Synthesis of graphene oxide and copper phthalocyanine. *J. Mater. Sci. Mater. Electron.* **32**, 886–893 (2021)
6. T. Guo, T. Xu, W. Xia, A.J. Carrier, L. Wang, X. Zhang, *Mater. Chem. Phys.* **260**, 124126 (2020)
7. M.Y.A. Rahman, A.S. Sulaiman, A.A. Umar, M.M. Salleh, J. Mater. Sci. Mater. Electron. **28**, 1674–1678 (2017)
8. S. Bae, H. Kim, Y. Lee, X. Xu, J.-S. Park, Y. Zheng, J. Balakrishnan, T. Lei, H.R. Kim, Y.I. Song, *Nat. Nanotechnol.* **5**, 574 (2010)
9. G. Jo, M. Choe, C.-Y. Cho, J.H. Kim, W. Park, S. Lee, W.-K. Hong, T.-W. Kim, S.-J. Park, B.H. Hong, *Nanotechnology* **21**, 75201 (2010)
10. L. Liu, F. You, Q. Zheng, B. Mo, B. Zeng, H. Wang, X. Zhang, B. Wei, *Phys. Status Solidi C.* **14**, 1600131 (2017)
11. M.M. Jaafar, P.C. Ooi, M.F. Mohd, R. Wee, M.A.S. Mohammad Haniff, M.A. Mohamed, E.Y. Chang, B. Yeop Majlis, C.F. Dee, *J. Mater. Sci. Mater. Electron.* **30**, 16415–16420 (2019)
12. D.R. Dreyer, S. Park, C.W. Bielawski, R.S. Ruoff, *Chem. Soc. Rev.* **39**, 228–240 (2010)
13. T. Li, T. Patel, I. Banerjee, R. Pearce-Hill, J. Gallop, L. Hao, A.K. Ray, *J. Mater. Sci. Mater. Electron.* **26**, 4810–4815 (2015)
14. J. Su, C. Li, *J. Mater. Sci. Mater. Electron.* **32**, 9065–9073 (2021)
15. S. Pei, J. Zhao, J. Du, W. Ren, H.-M. Cheng, *Carbon N. Y.* **48**, 4466–4474 (2010)
16. C. Fang, B. Dai, R. Hong, C. Tao, Q. Wang, X. Wang, D. Zhang, S. Zhuang, *Sci. Rep.* **5**, 15362 (2015)
17. F.M. El-Hossary, A. Ghitas, A.M. Abd El-Rahman, A.A. Ebnalwaled, M. Abdelhamid Shahat, *IOP Conf. Ser. Mater. Sci. Eng.* **956**, 012003 (2020). <https://iopscience.iop.org/article/10.1088/1757-899X/956/1/012003>
18. B. Jinnai, S. Fukuda, H. Ohtake, S. Samukawa, *J. Appl. Phys.* **107**, 43302 (2010)
19. T. Gokus, R.R. Nair, A. Bonetti, M. Bohmler, A. Lombardo, K.S. Novoselov, A.K. Geim, A.C. Ferrari, A. Hartschuh, *ACS Nano* **3**, 3963–3968 (2009)
20. K. Choi, J. Lim, J.R. Rani, H. Seo Yoon, J. Oh, T. Hong, T. Ha, B. Cheol Park, K. Ik Sim, S. Chan Jun, *Appl. Phys. Lett.* **102**, 131901 (2013)
21. M.N. Morshed, N. Bouazizi, N. Behary, J. Guan, V. Nierstraszc, *Chem. Eng. J.* **374**, 658–673 (2019)
22. H. Zhao, S. Fan, Y. Chen, Z. Feng, H. Zhang, W. Pang, D. Zhang, M. Zhang, *A.C.S. Appl. Mater. Interfaces.* **9**, 40774–40781 (2017)
23. M.-S. Chae, J. Kim, D. Jeong, Y. Kim, J.H. Roh, S.M. Lee, Y. Heo, J.Y. Kang, J.H. Lee, D.S. Yoon, *Biosens. Bioelectron.* **92**, 610–617 (2017)
24. Z. Ke, Y. Ma, Z. Zhu, H. Zhao, Q. Wang, Q. Huang, *Appl. Phys. Lett.* **112**, 13701 (2018)
25. A. Felten, A. Eckmann, J.J. Pireaux, R. Krupke, C. Casiraghi, *Nanotechnology* **24**, 355705 (2013)
26. S.J. Han, *IEEE Electr. Insul. Conf.* 529–532 (2018). <https://ieeexplore.ieee.org/document/8481096>
27. P.-G. Ren, D.-X. Yan, X. Ji, T. Chen, Z.-M. Li, *Nanotechnology* **22**, 55705 (2010)
28. M.J. McAllister, J.-L. Li, D.H. Adamson, H.C. Schniepp, A.A. Abdala, J. Liu, M. Herrera-Alonso, D.L. Milius, R. Car, R.K. Prud'homme, *Chem. Mater.* **19**, 4396–4404 (2007)
29. G. Williams, B. Seger, P.V. Kamat, *ACS Nano* **2**, 1487–1491 (2008)
30. P.J. Jesuraj, R. Parameshwari, K. Kanthasamy, J. Koch, H. Pfnür, K. Jeganathan, *Appl. Surf. Sci.* **397**, 144–151 (2017)
31. Y. Guo, W. Wang, S. Li, Y. Liu, T. Liu, Q. Wang, Q. Wang, X. Gao, Q. Fan, W. Li, *Solid. State. Electron.* **153**, 46–51 (2019)
32. N.I. Kovtyukhova, P.J. Ollivier, B.R. Martin, T.E. Mallouk, S.A. Chizhik, E.V. Buzaneva, A.D. Gorchinskiy, *Chem. Mater.* **11**, 771–778 (1999)
33. G. He, H. Chen, J. Zhu, F. Bei, X. Sun, X. Wang, *J. Mater. Chem.* **21**, 14631–14638 (2011)
34. F.M. El-Hossary, A. Ghitas, A.M. Abd El-Rahman, A.A. Ebnalwaled, M.H. Fawey, M.A. Shahat, *IOP Conf. Ser.: Mater. Sci. Eng.* **762**, 012001 (2020). <https://iopscience.iop.org/article/10.1088/1757-899X/762/1/012001>
35. S. Tang, S. Jin, R. Zhang, Y. Liu, J. Wang, Z. Hu, W. Lu, S. Yang, W. Qiao, L. Ling, *Appl. Surf. Sci.* **473**, 222–229 (2019)
36. V.K. Abdelkader-Fernández, M. Melguizo, M. Domingo-García, F.J. López-Garzón, M. Pérez-Mendoza, *Appl. Surf. Sci.* **464**, 673–681 (2019)
37. C.-R. Yang, S.-F. Tseng, Y.-T. Chen, *Appl. Surf. Sci.* **444**, 578–583 (2018)
38. C. Yang, J. Gong, P. Zeng, X. Yang, R. Liang, Q. Ou, S. Zhang, *Appl. Surf. Sci.* **452**, 481–486 (2018)
39. C.-M. Chen, Q. Zhang, M.-G. Yang, C.-H. Huang, Y.-G. Yang, M.-Z. Wang, *Carbon N. Y.* **50**, 3572–3584 (2012)

40. R. Arrigo, M. Hävecker, S. Wrabetz, R. Blume, M. Lerch, J. McGregor, E.P.J. Parrott, J.A. Zeitler, L.F. Gladden, A. Knop-Gericke, *J. Am. Chem. Soc.* **132**, 9616–9630 (2010)
41. I. Bertóti, M. Mohai, K. László, *Carbon N. Y.* **84**, 185–196 (2015)
42. Q. Yuan, S. Wu, C. Ye, X. Liu, J. Gao, N. Cui, P. Guo, G. Lai, Q. Wei, M. Yang, *Sens. Actuat. B Chem.* **285**, 333–340 (2019)
43. A.A. Pirzado, L. Truong-Phuoc, V. Papaefthimiou, C.M. Ghimbeu, F. Le Normand, H. Ba, T. Thanh-Tung, C. Pham-Huu, I. Janowska, *J. Colloid Interface Sci.* **451**, 221–230 (2015)
44. M. Aliofkhazraei, N. Ali, W.I. Milne, C.S. Ozkan, S. Mitura, J.L. Gervasoni (Taylorfrancis, Boca Raton, 2016), P. 42. <https://doi.org/10.1201/9781315374093>
45. K. Chu, Y. Liu, J. Wang, Z. Geng, Y. Li, *Mater. Sci. Eng. A.* **735**, 398–407 (2018)
46. Z. Li, Y. Xu, B. Cao, L. Qi, S. He, C. Wang, J. Zhang, J. Wang, K. Xu, *Superlattices Microstruct.* **99**, 125–130 (2016)
47. V.B. Mohan, R. Brown, K. Jayaraman, D. Bhattacharyya, *Mater. Sci. Eng. B.* **193**, 49–60 (2015)
48. I. Childres, L.A. Jauregui, J. Tian, Y.P. Chen, *New J. Phys.* **13**, 025008 (2010). <https://iopscience.iop.org/article/10.1088/1367-2630/13/2/025008> ()
49. I. Kondratowicz, M. Nadolska, S. Şahin, M. Łapiński, M. Przeźniak-Welenc, M. Sawczak, H.Y. Eileen, W. Sadowski, K. Żelechowska, *Appl. Surf. Sci.* **440**, 651–659 (2018)
50. A. Bajpai, R. Sharma, *Vacuum* **172**, 109033 (2020)
51. K.K.H. De Silva, H.-H. Huang, M. Yoshimura, *Appl. Surf. Sci.* **447**, 338–346 (2018)
52. J. Nicasio-Collazo, J.-L.L. Maldonado, J. Salinas-Cruz, D. Barreiro-Argüelles, I. Caballero-Quintana, C. Vázquez-Espinosa, D. Romero-Borja, *Opt. Mater. Amst.* **98**, 109434 (2019)
53. H. Feng, R. Cheng, X. Zhao, X. Duan, J. Li, *Nat. Commun.* **4**, 1–8 (2013)
54. S. Sakulsermsuk, P. Singjai, C. Chaiwong, *Diam. Relat. Mater.* **70**, 211–218 (2016)
55. W. Can, Z. Liang, W. Qiao, L. Ling, *New Carbon Mater.* **26**, 21–25 (2011)
56. D. Chen, H. Feng, J. Li, *Chem. Rev.* **112**, 6027–6053 (2012)
57. X. Dang, H. Zhao, X. Wang, T. Sailijiang, S. Chen, X. Quan, *Microchim. Acta.* **185**, 345 (2018)
58. J. Zhu, H. Deng, W. Xue, Q. Wang, *Appl. Surf. Sci.* **428**, 941–947 (2018)
59. J. Robertson, *Mater. Sci. Eng. R Reports.* **37**, 129–281 (2002)
60. N. McEvoy, H. Nolan, N.A. Kumar, T. Hallam, G.S. Duesberg, *Carbon N. Y.* **54**, 283–290 (2013)
61. F. Leroy, F. Müller-Plathe, *J. Chem. Phys.* **133**, 44110 (2010)
62. M. Psarski, D. Pawlak, J. Grobelny, G. Celichowski, *Appl. Surf. Sci.* **479**, 489–498 (2019)
63. S. Bronco, M. Bertoldo, E. Taburoni, C. Cepek, M. Sancrotti, in: *Macromol. Symp. Macromolecular Symposia*, **218**, 71–80 (2004). <https://onlinelibrary.wiley.com/doi/abs/10.1002/masy.200451408>
64. C. Arpagaus, A. Rossi, P.R. Von Rohr, *Appl. Surf. Sci.* **252**, 1581–1595 (2005)
65. I. Novak, Š Florián, Investigation of long-term hydrophobic recovery of plasma modified polypropylene. *J. Mater. Sci.* **39**, 2033–2036 (2004)
66. I. Novák, V. Pollak, I. Chodak, Study of surface properties of polyolefins modified by corona discharge plasma. *Plasma Process. Polym.* **3**, 355–364 (2006)
67. L. Yang, J. Chen, Y. Guo, Z. Zhang, *Appl. Surf. Sci.* **255**, 4446–4451 (2009)
68. D.K. Owens, R.C. Wendt, *J. Appl. Polym. Sci.* **13**, 1741–1747 (1969)
69. A. Carré, *J. Adhes. Sci. Technol.* **21**, 961–981 (2007)
70. P. Jia, F. Pan, T. Chen, *IOP Conf. Ser. Mater. Sci. Eng.* **182**, 12030 (2017). <https://iopscience.iop.org/article/10.1088/1757-899X/182/1/012030/meta>
71. M. Ishigami, J.H. Chen, W.G. Cullen, M.S. Fuhrer, E.D. Williams, *Nano Lett.* **7**, 1643–1648 (2007)
72. K.V. Rani, B. Sarma, A. Sarma, *Diam. Relat. Mater.* **84**, 77–85 (2018)
73. S.M. Hafiz, R. Ritikos, T.J. Whitcher, N.M. Razib, D.C.S. Bien, N. Chanlek, H. Nakajima, T. Saisopa, P. Songsiriritthigul, N.M. Huang, *Sens. Actuat. B Chem.* **193**, 692–700 (2014)
74. A. Mathkar, D. Tozier, P. Cox, P. Ong, C. Galande, K. Balakrishnan, A. LeelaMohanaReddy, P.M. Ajayan, *J. Phys. Chem. Lett.* **3**, 986–991 (2012)

**Publisher's Note** Springer Nature remains neutral with regard to jurisdictional claims in published maps and institutional affiliations.